J Ther Eng, Vol. 11, No. 3, pp. 765–779, May, 2025

Journal of Thermal Engineering
Web page info: https://jten.yildiz.edu.tr
DOI: 10.14744/thermal.0000945

Research Article

Heat and mass transfer analysis of unsteady MHD Carreu Nanofluid flow over a stretched surface in a porous medium with Stefan blowing condition

R. GEETHA[1], B. REDDAPPA[1,*], A. SUMITHRA[1], B. RUSHI KUMAR[2], B. PRABHAKAR REDDY[3]

[1]*Department of Mathematics, Kalasalingam Academy of Research and Education (Deemed to be University), School of Advanced Sciences, Tamil Nadu, 626126, India*
[2]*Department of Mathematics, Vellore Institute of Technology, School of Advanced Sciences, Tamil Nadu, 632014, India*
[3]*Department of Mathematics and Statistics, The University of Dodoma, Dodoma, 41218, Tanzania*

ARTICLE INFO

Article history
Received: 01 April 2024
Revised: 06 July 2024
Accepted: 07 July 2024

Keywords:
Carreau Nanofluid; Heat Transfer; MHD; Porous Medium; Stefan Blowing; Unsteady Flow

ABSTRACT

This study delves into the magneto-hydrodynamic (MHD) flow of a non-Newtonian nanofluid over an unstable stretched surface, focusing on the effects of suction and Stefan blowing. Employing innovative approaches, such as modeling the nanofluid as a two-phase system and using the Carreau fluid model for non-Newtonian behavior, the research generates a numerical solution for heat and mass transfer analysis of unsteady MHD Carreau nanofluid flow in a porous medium under Stefan blowing conditions. By applying similarity transformations, the Carreau fluid flow equations are converted into dimensionless non-linear ordinary differential equations, which are then solved using MATLAB›s bvp4c function. The study meticulously examines the influence of various dimensionless parameters on mass transfer, temperature, concentration, friction factor, and dimensionless velocity, with results presented through comprehensive graphs and tables. Key findings indicate that both temperature and fluid velocity increase with higher Stefan blowing/suction parameters, while temperature decreases with rising fluid velocity and Weissenberg number. These insights are crucial for enhancing the performance and longevity of critical machinery, such as bearings, sliding components, and engines. The study highlights Stefan blowing›s potential to boost heat transfer efficiency by reducing thermal resistance and improving the heat transfer coefficient. The synergistic effects of Carreau nanofluid and Stefan blowing offer promising applications in cooling systems, thermal management tools, and lubrication within the oil and gas industry. The findings advance thermal management technologies and provide a new perspective on engineering applications across various sectors. The range of some physical parameters which are used in this study are: The power-law index ($0<n<2$), Weissenberg Number ($0< We< 100$), Magnetic Parameter ($0<M< 100$), Prandtl Number (Gases: $0.7<Pr< 1$, Liquids: $1<Pr<100$, Oils: $100<Pr<10{,}000$), Lewis Number ($0.01<Le<10$).

Cite this article as: Geetha R, Reddappa B, Sumithra A, Rushi Kumar B, Prabhakar Reddy B. Heat and mass transfer analysis of unsteady MHD Carreu Nanofluid flow over a stretched surface in a porous medium with Stefan blowing condition. J Ther Eng 2025;11(3):765–779.

*Corresponding author.
*E-mail address: drbreddappa@gmail.com

This paper was recommended for publication in revised form by Editor-in-Chief Ahmet Selim Dalkılıç

Published by Yıldız Technical University Press, İstanbul, Turkey

INTRODUCTION

Nanofluids are increasingly widely employed in a wide range of industries because they include nanoparticles smaller than 100 nm, which improve heat conductivity. These sectors include the following: aggregate production, heat exchangers, solar collectors, pharmaceutical operations, reactors, absorption technologies, refrigerator chiller systems, and coolant applications [1–8]. Furthermore, new disciplines including brain tumor therapy, heart surgery, cancer treatment, and safe cooling techniques have found a use for nanofluids. The groundwork for the research of nanofluids was laid by the groundbreaking studies of Masuda et al. [9] and Choi [10], which focused on the dispersion of ultrafine particles constantly suspended in a base fluid. Boundary layer flow and nanoparticle dispersion in a microchannel in the presence of a magnetic field was investigated by various researchers [11-15].

In addition to nanofluids, fluid flow through porous media plays a crucial role in various engineering fields including geothermal, petroleum, and industrial engineering. Porous media consists of a solid matrix with interconnected pores that enable fluid movement, encompassing natural materials like sand, wood, and human lungs, as well as synthetic materials such as ceramics, composite materials, and high-porosity metal foams. Porous media finds applications in micro-chemical reactors, steel and iron manufacturing, electrochemical systems, and renewable fuel generation. The study of porous media has traditionally relied on Darcy›s law for theoretical and computational analyses.

Heat transmission and fluid flow phenomena in porous media have been the subject of several studies. In their investigation of triple diffusive flow saturated by nanofluid across a permeable horizontal plate, Khan et al. [16] showed that the inclusion of salts and nanoparticles increases heat transfer rates. Convection dominates heat transfer at high porosity and conduction at low porosity, according to Krishna and Reddy›s [17] analysis of MHD non-Newtonian forced convective flow across the porous medium. The effects of MHD slip flux and heat transfer across a permeable stretched sheet were investigated by Hayat et al. [18]. Furthermore, several researchers [19–24] have looked at how different fluid types affect MHD flow in a variety of geometries.

One important non-Newtonian fluid model that well depicts the processes of shear thinning and thickening is the Carreau fluid flow model. “It offers a thorough grasp of the rheological behavior of several industrial fluids, including detergents used in biotechnology, syrups, foams, and cosmetics. There have been several investigations into the various aspects of Carreau fluid flow in the past, such as the following: incompressible Carreau fluid flow in an asymmetric channel with modified wall shapes [25], free convective layer flow around a heated vertical plate in a porous medium [26], stagnation flow to a flat plate [27], MHD boundary layer flow over a moving stretch surface in a porous medium [28], and thermal convection and mass transport in Carreau magnetohydrodynamic (MHD) fluid along a vertical porous plate [29], among others. Several noteworthy works in the field of fluid dynamics research have advanced our knowledge of a variety of flow phenomena. The MHD peristaltic flow of Carreau liquid in a channel was studied by Hayat et al. [30], who focused on analyzing different waveforms. To shed light on its behavior, Akbar et al. [31] investigated the two-dimensional flow of stagnation for an incompressible Carreau fluid across a diminishing surface. Suneetha and Gangadhar [32] built on Akbar›s work by including the MHD effect and convective boundary conditions in their analysis.

Moving on to the consideration of mass and heat transfer, Abou-Zeid [33] performed a computer study of the MHD flow of Carreau fluids across non-Darcy porous media while taking chemical reactions and diffusion into account. To better understand the behavior of the peristaltic flow of Carreau micro liquid in an asymmetric channel, Akbar et al. [34] conducted research. Furthermore, Akbar and Nadeem [35] examined the peristaltic flow of Carreau fluid in a uniform tube while accounting for long wavelength effects and taking mass and heat transfer into consideration. Nandeppanavar et al. [36] studied the flow and heat transmission of MHD fluids over an impermeable stretched surface by examining the effects of magnetic fields on heat transfer. They took into account several variables, including immersion, non-uniform heat sources, and fluctuating thermal conductivity. They also considered partial slip situations. Chiam [37] examined how a linearly stretched sheet affected heat flow and transmission while accounting for differences in thermal conductivity. Cortell [38] carried out a quantitative investigation on the flow and heat transfer in a viscous fluid approaching a non-linear stretched sheet in the setting of non-linear stretching sheets. The effects of heat radiation and dissipation on the flow of the MHD boundary layer and heat transfer across non-linear stretching sheets were investigated by Vyas and Ranjan [39]. Additionally, Ali [40] examined the effects of a thermal boundary layer, injection, and suction on a power law stretching sheet. Several researchers have been reported to predict the characteristics of MHD nanofluid [41–45], Transient nanofluid squeezing cooling process using aluminum oxide nanoparticle [46].

A Carreau nanofluid is a type of non-Newtonian fluid that follows the Carreau model, which describes how the viscosity of the fluid changes with the rate of shear strain. Although the Carreau fluid model has been investigated in great detail, the MHD flow of Carreau nanofluids over a stretched sheet when Stefan blowing is present has not received as much attention. Stefan blowing refers to the mass transfer process where a phase change occurs at a boundary, leading to the ejection (blowing) or absorption (suction) of mass through that boundary. It has been discovered that Stefan blowing significantly affects lubricating systems, improving the longevity and performance of industrial elements including engines, sliding parts, and bearings. Furthermore, Stefan blowing may efficiently lower thermal resistance and raise the heat transfer coefficient in heat exchangers and cooling systems. Thus, investigating how Stefan blowing and Carreau nanofluids work together to improve heat transmission is a fresh and exciting line of inquiry.

The Prandtl number (Pr) is a dimensionless number that relates the momentum diffusivity (viscous diffusion) to the thermal diffusivity. It essentially provides a measure of the relative thickness of the momentum and thermal boundary layers. The Prandtl number is defined as: $Pr = \frac{v}{\alpha}$ where v is the kinematic viscosity and α is the thermal diffusivity.

The Nusselt number (Nu) is the ratio of convection heat transfer to conduction heat transfer across the boundary. The Nusselt number is defined as: $Nu = \frac{hL}{k}$ where h is the convective heat transfer coefficient, L is a characteristic length (such as the length of a plate or diameter of a pipe) and k is the thermal conductivity of the fluid.

This work aims to explore the mass and heat transfer characteristics of the MHD Carreau nanofluid flow across an unstable stretching surface when Stefan blowing is present. The governing equations are converted into ordinary equations by using similarity transformations, and then the Matlab solver bvp4c is used to solve the equations numerically. Temperature, velocity, and concentration effects of pertinent factors in the blowing/suction situations are investigated, and the findings are graphically shown using graphs. Furthermore, further calculations and analyses are carried out to assess skin friction, Sherwood and Nusselt numbers, and other pertinent physical characteristics. Our goal is to further our knowledge of the intricate interactions of heat transfer, Stefan blowing, and Carreau nanofluids." The design and optimization of cooling strategies, lubrication systems, and thermal management systems in a variety of sectors are affected by the study›s conclusions.

MATHEMATICAL FORMULATION AND PHYSICAL MODEL

We"study a two-dimensional unsteady Carreau nanofluid flow traveling at a velocity $U(x,t) = \frac{ax}{1-at}$ over a stretched exterior, where t is the time, α is a positive constant, and a > 0 is any constant. Darcy›s law is applied to porous media, and the flow is limited to the region where $y \geq 0$. Across the y-axis, a transverse uniform magnetic force B_0 is applied. Figure 1 displays a sketch of the physical flow problem. The magnetic and electric fields follow the law of Ohm's $J = \sigma(E + V \times B_0)$, where V, J and σ represent the velocity of the fluid, Joule current, and the electrical conductivity, respectively. The Joule (current) effect mentioned also plays a role in the transport of a charged particle in the electromagnetic field. Since the magnetic Reynolds number is small, the induced magnetic field and Hall current effects are ignored. The impacts of Stefan blowing have also been considered. Assuming the velocity of the linearly stretching sheet is $U = (x,t)$, where the x-axis and y-axis are assumed along the stretched sheet. Suppose that the values of the ambient concentration and temperature are symbolized by (C_∞ and T_∞), respectively. It is also assumed that the temperature and concentration at the surface have a constant value of T_W and C_W.

Buongiorno›s nanofluid model is used to tackle this nanofluid flow model. This model›s base fluid has nanoparticles in it that are between 10 and 100 nm in size. In these cases, the nanoparticles are in the solid phase and the base fluid is in the liquid phase. Nanoparticles suspended in a base fluid do affect the thermophysical properties of the resulting nanofluid, such as viscosity, density, thermal conductivity, and specific heat capacity. The presence of nanoparticles, even in the solid phase, changes the overall properties of the nanofluid compared to the base fluid alone. However, the nanoparticles themselves do not affect the properties of the base fluid, as they are dispersed within the base fluid in the solid phase. Rather, the random motions of nanoparticles lead to thermophoresis effects and Brownian motion, which have a significant influence on heat and mass transport. As a result, any kind of nanoparticle with a diameter of 10–100 nm, including Ag, CuO, Al_2O_3, and others, applicable with this fluid model.

The thermophysical properties of nanofluid flow modeled using the Buongiorno model, which accounts for both Brownian motion and thermophoresis, can be described as follows:

Density (ρ)

The density of the nanofluid is typically a function of the base fluid density (ρ_f), nanoparticle density (ρ_p), and nanoparticle volume fraction (φ). The nanofluid density $\rho = (1 - \varphi)\, \rho_f + \varphi\rho_p$.

Dynamic Viscosity (μ)

The dynamic viscosity of the nanofluid can be influenced by factors such as the base fluid viscosity, nanoparticle size, and nanoparticle volume fraction.

Thermal Conductivity (k)

The thermal conductivity of the nanofluid is generally higher than the base fluid due to the presence of the nanoparticles.

Specific Heat Capacity (C_p)

The specific heat capacity of the nanofluid can be calculated using the mixture formula: $c_p = (1 - \varphi)\,(c_p)_f + \varphi(c_p)_p$, where $(c_p)_f$ and $(c_p)_p$ are the specific heat capacities of the base fluid and nanoparticles, respectively.

Brownian Motion

Brownian motion refers to the random movement of nanoparticles due to their collision with the surrounding fluid molecules. Brownian motion can enhance the heat transfer and mass diffusion in the nanofluid. The Buongiorno model incorporates the effects of Brownian motion through a term in the energy and species transport equations.

Thermophoresis

Thermophoresis is the phenomenon where nanoparticles migrate from the hotter regions to the colder regions of the fluid due to the temperature gradient. Thermophoresis can also contribute to the heat transfer and mass diffusion in the nanofluid. The Buongiorno model includes the effects of thermophoresis through a term in the species transport equation.

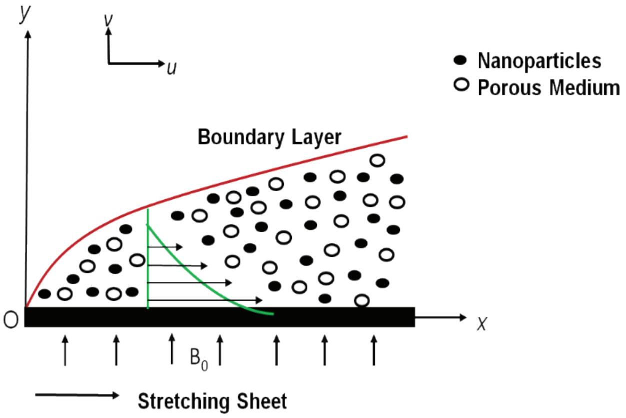

Figure 1. Flow geometry.

In the examination of motion, the partial differential equations overriding the fluid motion, heat, and mass transport are [47, 48].

$$\frac{\partial u}{\partial x}+\frac{\partial v}{\partial y}=0 \tag{1}$$

$$\frac{\partial u}{\partial t}+u\frac{\partial u}{\partial x}+v\frac{\partial u}{\partial y}=\nu\left[\frac{\partial^2 u}{\partial y^2}+\frac{3(n-1)}{2}\Gamma^2\frac{\partial^2 u}{\partial y^2}\left(\frac{\partial u}{\partial y}\right)^2\right]-u\left(\frac{\sigma {B_0}^2}{\rho}+\frac{\nu}{k_1}\right) \tag{2}$$

$$\frac{\partial T}{\partial t}+u\frac{\partial T}{\partial x}+v\frac{\partial T}{\partial y}=\alpha\frac{\partial^2 T}{\partial y^2}+\frac{(\rho c_p)_p}{(\rho c_p)_f}\left[D_B\frac{\partial C}{\partial y}\frac{\partial T}{\partial y}+\frac{D_T}{T}\left(\frac{\partial T}{\partial y}\right)^2\right] \tag{3}$$

$$\frac{\partial C}{\partial t}+u\frac{\partial C}{\partial x}+v\frac{\partial C}{\partial y}=D_B\frac{\partial^2 C}{\partial y^2}+\frac{D_T}{T_\infty}\frac{\partial^2 T}{\partial y^2}-C_r(C-C_\infty) \tag{4}$$

The appropriate boundary conditions for this problem are given below,

$$u=U(x,t), v=-\frac{D_B}{1-C_W}\frac{\partial C}{\partial y}, T=T_W, C=C_W \text{ at } y=0 \tag{5}$$

$$u\to 0, T\to T_\infty, C\to C_\infty \text{ as } y\to\infty \tag{6}$$

Similarity transformations

$$\psi=x\sqrt{\frac{a\nu}{1-\alpha t}}f(\eta), \eta=y\sqrt{\frac{a}{\nu(1-\alpha t)}}, \theta(\eta)=\frac{T-T_\infty}{T_W-T_\infty},$$
$$\phi(\eta)=\frac{C-C_\infty}{C_W-C_\infty} \tag{7}$$

Where ψ represents stream function and is expressed by the following relation

$$u=\frac{\partial\psi}{\partial y}, v=-\frac{\partial\psi}{\partial x} \tag{8}$$

We get the next arrangement of nonlinear ordinary differential equations:

$$f'''-f'^2+ff''+\frac{3(n-1)}{2}We^2f''^2f'''-A\left(\frac{\eta}{2}f''+f'\right)$$
$$-(M^2+\lambda)f'=0 \tag{9}$$

$$\frac{1}{Pr}\theta''-\frac{A}{2}\eta\theta'+f\theta'+Nb\theta'\phi'+Nt\theta'^2=0 \tag{10}$$

$$\frac{1}{Le}\phi''-\frac{A}{2}\eta\phi'+f\phi'+\frac{1}{Le}\frac{Nt}{Nb}\theta''-\gamma\phi=0 \tag{11}$$

where $A=\frac{\alpha}{a}$ represents the unsteadiness parameter, $Pr=\frac{\nu}{\alpha}$ denotes the Prandtl number, $Nb=\frac{(\rho c_p)_p D_B(C_W-C_\infty)}{(\rho c_p)_f \nu}$ represents the Brownian motion Parameter, $Nt=\frac{(\rho c_p)_p D_T(T_W-T_\infty)}{(\rho c_p)_f T_\infty \nu}$ represents the thermophoresis parameter, $Le=\frac{\nu}{D_B}$ denotes the Lewis number, $We^2=\frac{\Gamma^2a^3x^2}{\nu(1-\alpha t)^3}$ represents the Weissenberg number, $\lambda=\frac{\nu(1-\alpha t)}{ak_1}$ is the Porosity parameter, $M^2=\frac{\sigma {B_0}^2(1-\alpha t)}{a\rho}$ is the Hartmann number, $\gamma=\frac{C_r(1-\alpha t)}{a}$ Chemical reaction parameter.

The criteria for the boundaries:

$$f'(\eta)=1, f(\eta)=\frac{S}{Le}\phi'(\eta), \theta(\eta)=1, \phi(\eta)=1 \; when\; \eta=0 \tag{12}$$

$$f'(\eta)=0, \theta(\eta)=0, \phi(\eta)=0 \; as\; \eta\to\infty \tag{13}$$

Here $S=\frac{C_W-C_\infty}{1-C_W}$ denotes the Stefan blowing parameter ($S > 0$ represents blowing and $S < 0$ represents suction).

Three fundamental physical attributes are considered: the Sherwood number, the Nusselt number, and the skin-friction coefficient:

$$C_f=\sqrt{Re_x}\left[\frac{\mu}{\rho U^2}\left(\frac{\partial u}{\partial y}\right)_{y=0}\right], \; Nu=\left[\frac{xk}{\sqrt{Re_x}}\left(\frac{\partial T}{\partial y}\right)_{y=0}\right],$$
$$Sh=\left[\frac{xD_B}{\sqrt{Re_x}}\left(\frac{\partial C}{\partial y}\right)_{y=0}\right] \tag{14}$$

Substituting Eq. (7) and (8) into (14) to obtain the final dimensional form:”

$$\sqrt{Re_x}C_f=f''(0), \; Nu=-\theta'(0), \; Sh=-\phi'(0) \tag{15}$$

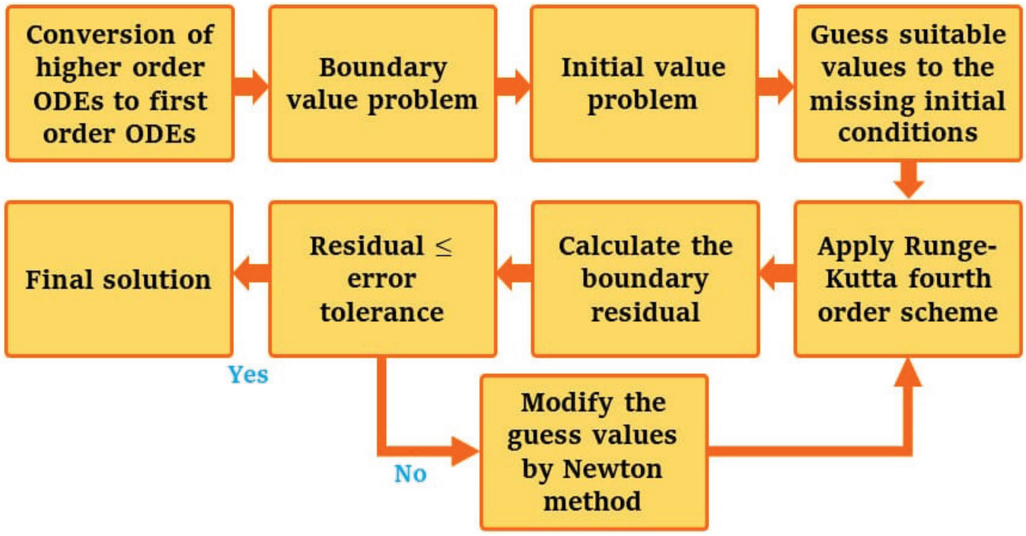

Figure 2. Step-by-step numerical procedure.

where $Re_x = \frac{ax^2}{\upsilon(1-\alpha t)}$ stands for the local Reynolds number, C_f the local skin friction, *Nu* the local Nusselt number, and *Sh* the local Sherwood number.

Numerical Solution Procedure

The BVP4c technique is a numerical method used to solve boundary value problems (BVPs). BVP involves finding a solution to a differential equation that satisfies specified boundary conditions. The BVP4c technique provides a robust and efficient way to solve BVPs numerically. By discretizing the problem, formulating and solving the resulting system of equations, and incorporating the specified boundary conditions (Fig. 2).

Higher-order differential equations can be made into linear equations by adding more variables.

$$f_1=f, f_2=f', f_3=f'', f_4=\theta, f_5=\theta', f_6=\phi, f_7=\phi' \quad (16)$$

The first-order ODE that follows is obtained by transforming equations (9) through (11)

$$f'_2=f_3, f'_3=\frac{-2}{2+[3(n-1)Wef_3{}^2]}\left(f_1f_3-f_2{}^2-A\left(\frac{\eta}{2}f_3+f_2\right)-(M^2+\lambda)f_2\right) \quad (17)$$

$$f'_4=f_5, f'_5=-Pr\left(f_1f_5-\frac{A}{2}\eta f_5+Nbf_5f_7+Ntf_5{}^2\right) \quad (18)$$

$$f'_6=f_7, f'_7=-Le\left(f_1f_7-\frac{A}{2}\eta f_7+\frac{Nt}{LeNt}f_7-\gamma f_6\right) \quad (19)$$

with the boundary conditions:

$$f_a(1)=\frac{Sf_a(7)}{Le}, f_a(2)=1, f_a(4)=1, f_a(6)=1, \\ f_b(2)=0, f_b(4)=0, f_b(6)=0 \quad (20)$$

Numerical results for the approximate solutions are produced by MATLAB bvp4c programming, and these results show the physical significance of the non-dimensional constraints.

Code Validation

In Table 1, we compared our results of the Nusselt number -$\theta'(0)$ for different values of the parameter *Pr* when $S = M = We = \lambda = 0$ with the works of Grubka and Bobba [49] and Saheb Konai et al. [50] and observed a tremendous correlation among the results. Table 2 exhibits perfect agreement between $f''(0)$ the results of Oyelakin et al. [51], Sharidan et al. [52], Mukhopadhyay et al. [53], and Konai et al. [54] for a range of data regarding the parameter

Table 1. Values of -$\theta'(0)$ various values of Prandtl number *Pr*

Pr	Grubka and Bobba [49]	Konai et al. [50]	Present results for ordinary viscous fluid (for A=S=M=We=λ=0)
0.72	0.4631	0.463145	0.463124
1.00	0.5820	0.582011	0.582035
3.00	1.1652	1.165240	1.165464
10.00	2.3080	2.308000	2.308041
100.00	7.7657	7.765650	7.765660

Table 2. Values of $f''(0)$ various values of unsteadiness parameters A for an ordinary viscous fluid

A	Oyelakin et al. [51]	Sharidan et al. [52]	Mukhopadhyay et al. [53]	Konai et al. [54]	Present results
0.8	-1.261043	-1.261042	-1.261479	-1.26106	-1.261043
1.2	-1.377725	-1.377722	-1.3778062	-1.37774	-1.377725

associated with unsteadiness for viscous incompressible Newtonian liquid in the nonappearance of Stefan blowing/suction.

RESULTS AND DISCUSSION

For various flow parameters, including the power index n, the Weissenberg number We, the unsteadiness parameter A, the magnetic parameter WM, the porosity parameter λ, the Prandtl number Pr, the Brownian motion parameter Nb, the thermophoresis parameter Nt, the Lewis number Le, the chemical reaction parameter γ, the Stefan blowing/suction parameter S, we will discuss the numerical results of the dimensionless concentration, velocity, and temperature profiles in this article. All other parameters remain constant, except the chosen physical parameters, which are altered. These include: $M = 0.5$, $We = 0.3$, $A = 0.7$, $Le = 0.5$, $\lambda = 0.5$, $n = 0.5$, $Pr = 0.7$, $Nb = 0.2$, $Nt = 0.1$, $\gamma = 0.1$

The differences in dimensionless velocity, temperature, and concentration profiles concerning n are shown in Figure 3(a)–(c). These data confirm that the velocity and concentration decrease with increasing n, but the temperature distribution behaves oppositely for both the Stefan blowing/suction instances. This is because the power-law index increases the resistive force and, as a result, the fluid's non-Newtonian behavior by decreasing the sheet's non-linearity. The effects We are shown in Figure 4(a)-(c), which shows how velocity, temperature, and concentration profiles are affected. It is evident that while velocity increases with an increase in We, temperature and concentration profiles decrease in both the Stefan blowing/suction cases." This indicates that the effect is positive in that the fluid moves more quickly as a result of an increase in the coefficient's values. The contours of temperature, concentration, and velocity for a range of values of A are shown in Figure 5(a)–(c). The initial speed of the liquid increased as A expanded, as seen in Figure 5(a). According to this result, A is probably the cause of the thicker momentum boundary layer in Stefan's blowing/suction. In both the Stefan blowing/suction scenarios, the temperature increases the mounting data value for A, as seen in Figure 5(b). Furthermore, the fluid cooling rate is shown to be more efficient for Stefan suction than blowing. For both Stefan blowing and suction Figure 5(c), concentration amplifies the value of mounting data of A. Figure 6(a)-(c) display the parameter M on velocity, temperature, and concentration respectively. It is noticed that concentration profiles and velocity trends show an augmenting trend in temperature and velocity with increasing M. The strong Lorentz force that is produced as a result of the increase θ causes the fluid flow to slow down because it creates more resistance temperature, which is increased for both Stefan blowing/suction. The impact of λ in velocity, temperature, and concentration for both Stefan blowing/suction is shown in Figure 7(a)-(c). As seen in Figure 7(a), the velocity profile decreases with λ. This is because increases the fluid's resistances because of Darcian drag. The impact on temperature is seen in Figure 7(b). The temperature is seen to be rising as the porosity parameter λ rises. Concentration profiles are seen in Figure 7(c) as a result of λ higher mass diffusivity. The temperature, velocity, and concentration contour fluctuations for similar data for S are shown in Figure 8(a)–(c). The fluid velocity increases for both steady and unsteady flows, as illustrated in Figure 8(a) when the increasing values for the Stefan suction/blowing parameter S diverge. The trick to reviving species spread is to disperse little primitives over the barrier. However, when tiny particles are delivered, dispersion slows down, increasing the liquid's velocity as injection values rise. For both uneven and constant flows, temperature increases with increasing values of the Stefan suction/blowing parameter S, as shown in Figure 8(b). The concentration increases as the size of the data for S increases, as seen in Figure 8(c). The impact of Pr the temperature and concentration fields for the Stefan blowing/suction situations is depicted in Figures 9(a)–(b). The inverse connection between Pr the fluid's thermal diffusivity explains this particular behavior, which is observed in Figure 9(a). "Less thermal diffusion is indicated by a greater Pr, which further suggests a lower temperature is seen. Figure 9(b) shows that the concentration rises more quickly for Stefan blowing than for suction for increasing values of Pr. The effects of Nb is shown in Figure 10(a)–(b), where it can be seen that increasing Nb causes an enhancement in the thermal boundary level width (Fig. 10(a)). A diminishing concentration trend is seen in Figure 10(b), where increasing data for Nb is observed for both Stefan blowing/suction. When Nb increases and the fluids collide more frequently, a disorderly movement of nanoparticles develops. The effect of Nt on temperature and concentration profiles for both Stefan blowing/suction is shown in Figure 11(a)-(b). As Nt levels rise, so do temperature profiles. The transport force known as thermophoresis is brought about by the fluid's layers temperature gradient. Increases in the thermophoresis parameter indicate that the concentration profiles show the opposite behavior, with an increase in the temperature differential between the layers translating into an increase in the heat transformation rate. Figure 12 and 13, respectively, show concentration curves that decline as data for Le and γ rise under both Stefan blowing/suction."

Table 3 displays the values for the skin friction coefficient, Nusselt number, and Sherwood number for a range of relevant parameter values. As the power index n, magnetic parameter M, and porosity parameter λ increase, it can be seen that the skin friction coefficient, Nusselt number, and Sherwood number drop. For higher n typically means higher viscosity at higher shear rates, leading to decreased skin friction, Nusselt, and Sherwood numbers. Higher M usually increases the resistance to fluid motion (due to magnetic damping), reducing skin friction, Nusselt, and Sherwood numbers. For higher porosity decreases the effective surface area for heat and mass transfer, leading to lower skin friction, Nusselt, and Sherwood numbers. While the Weissenberg number We shows the opposite trend. For higher We increases fluid elasticity, which can enhance the resistance to deformation, leading to increased skin friction but potentially higher rates of heat and mass transfer. Research indicates that an increase in the unsteadiness parameter A, Stefan blowing/suction parameter S, the skin friction coefficient results in an increase; however, the trend is the opposite for the Sherwood number and the Nusselt number. An increase in A can increase the skin friction coefficient due to the additional inertia effects but can decrease the Nusselt and Sherwood numbers due to the instability in boundary layers. The skin friction coefficient and Nusselt number are thought to decrease as the Lewis number Le rises, while the Sherwood number shows the reverse pattern. For higher Le implies that heat diffuses faster than mass. This typically decreases skin friction and Nusselt numbers but increases the Sherwood number. Observations reveal that the Nusselt number rises as the Prandtl number Pr rises, while the Sherwood number shows the opposite pattern. For higher Pr indicates a thicker thermal boundary layer relative to the velocity boundary layer, increasing the Nusselt number but decreasing the Sherwood number. It is evident that when the parameters for chemical reactions γ, thermophoresis Nt, and Brownian motion Nb rise, the Nusselt number drops, while the Sherwood number exhibits the opposite tendency. It shows that for higher γ can reduce the Nusselt number due to the exothermic or endothermic nature of reactions, while increasing the Sherwood number as mass transfer is enhanced by chemical reactions. For higher Nt can decrease the Nusselt number as heat is carried away by particles, while increasing the Sherwood number due to enhanced mass transfer. For higher Nb increases the random movement of particles, reducing the Nusselt number but enhancing the Sherwood number due to increased mass transfer.

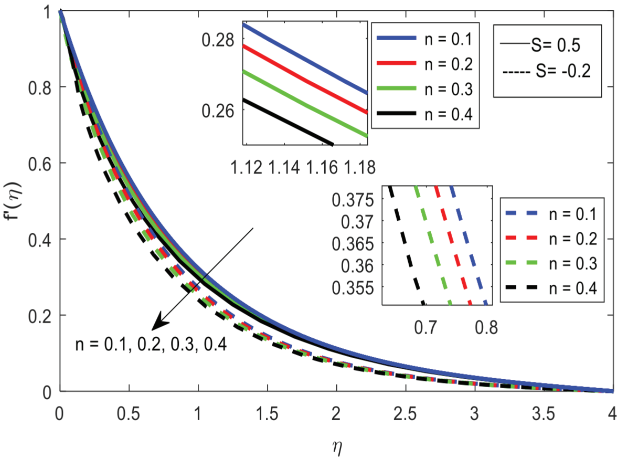

Figure 3(a). $f'(\eta)$ Profiles for various n values.

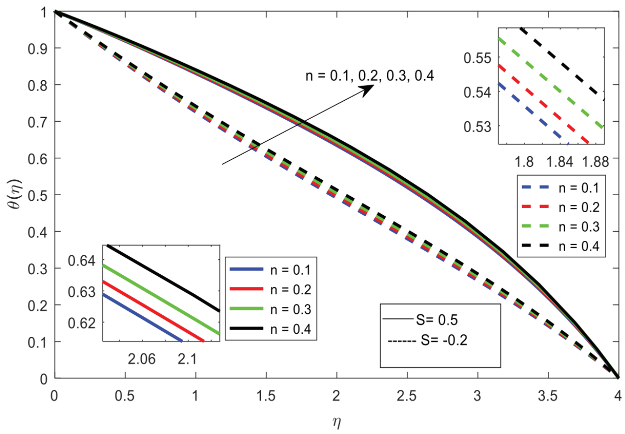

Figure 3(b). $\theta(\eta)$ Profiles for various n values.

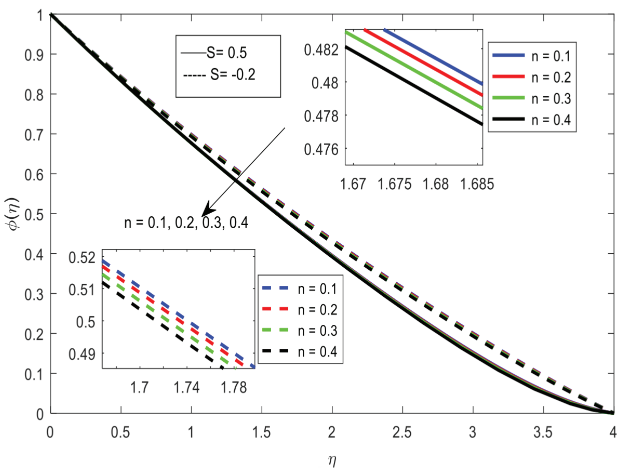

Figure3 (c). $\phi(\eta)$ Profiles for various n values.

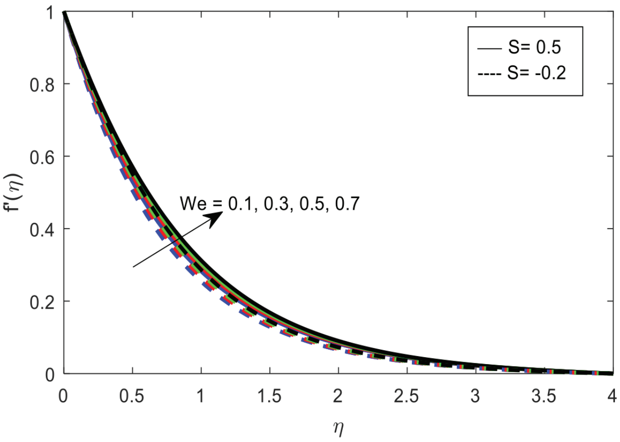

Figure 4(a). $f'(\eta)$ Profiles for various *We* values.

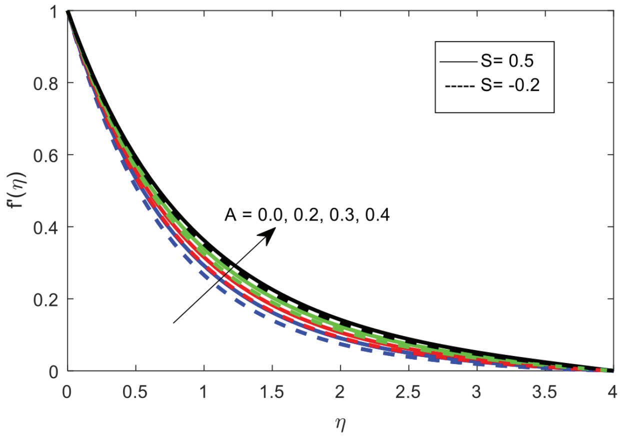

Figure 5(a). $f'(\eta)$ Profiles for various *A* values.

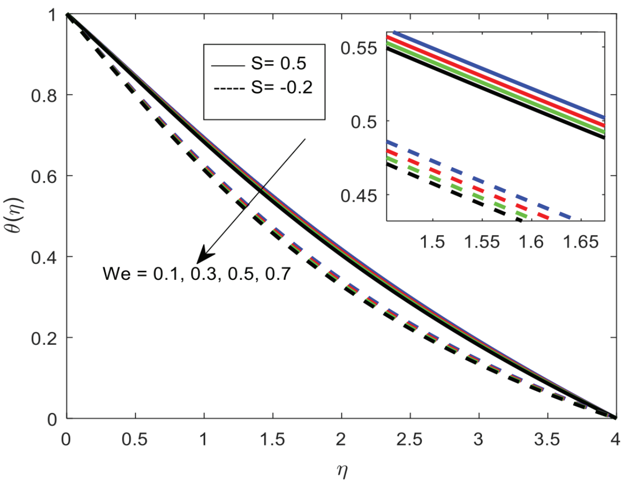

Figure 4(b). $\theta(\eta)$ Profiles for various *We* values.

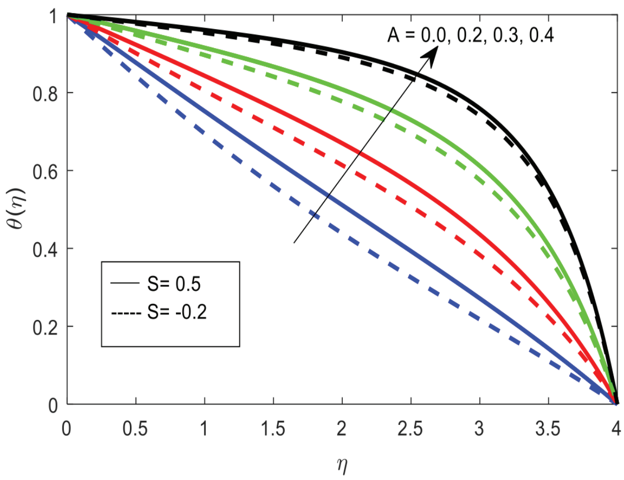

Figure 5(b). $\theta(\eta)$ Profiles for various *A* values.

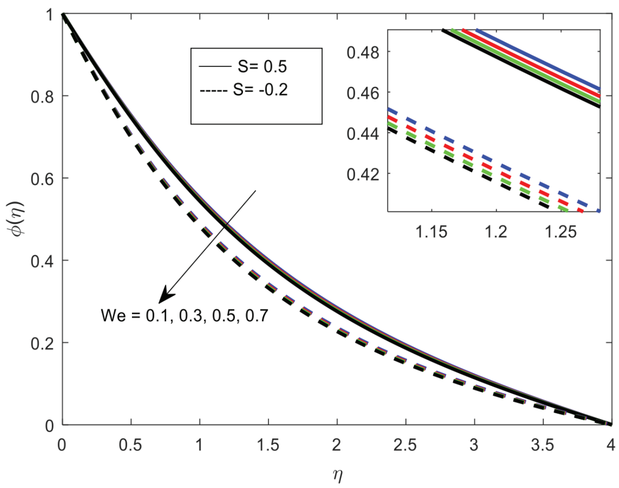

Figure 4(c). $\phi(\eta)$ Profiles for various *We* values.

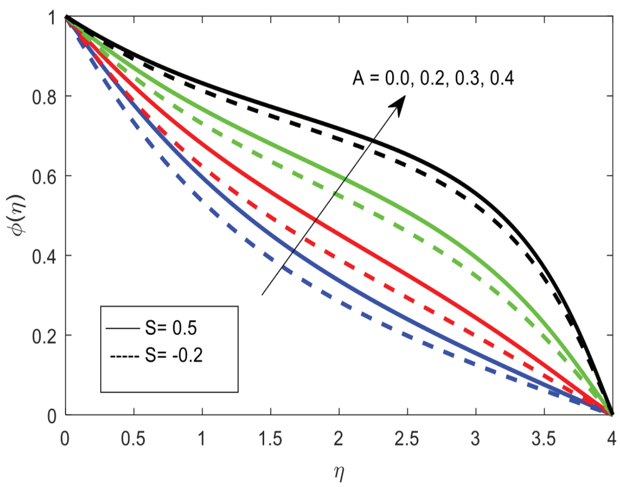

Figure 5(c). $\phi(\eta)$ Profiles for various *A* values.

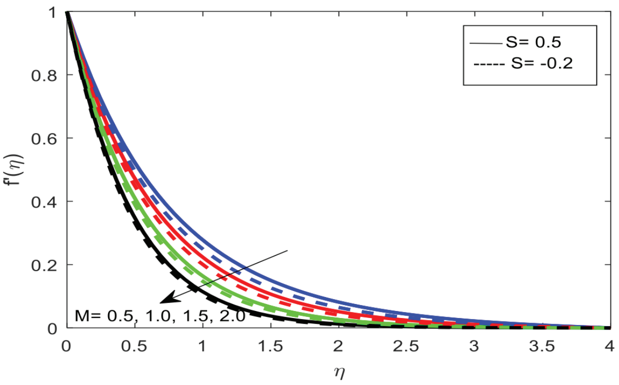

Figure 6(a). $f'(\eta)$ Profiles for various M values.

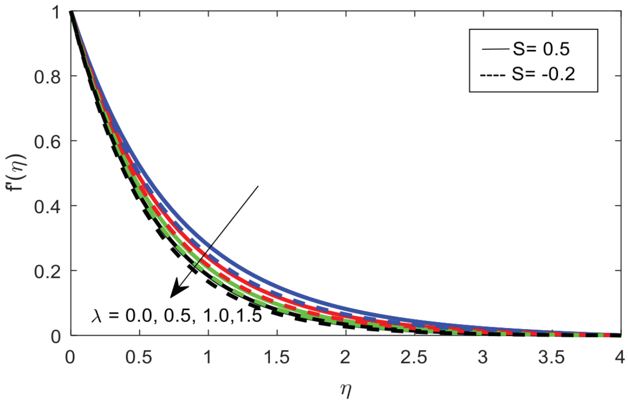

Figure 7(a). $f'(\eta)$ Profiles for various λ values.

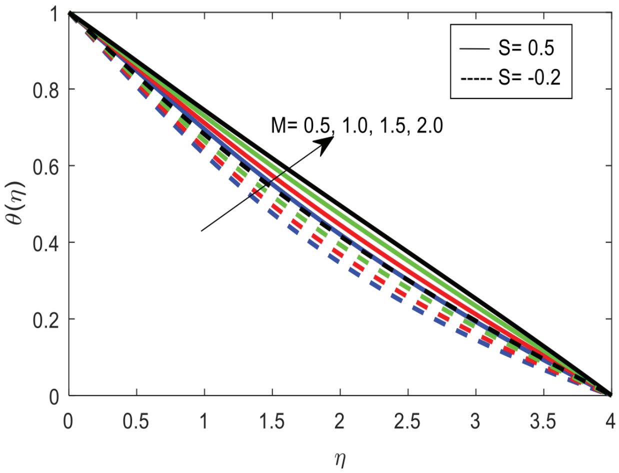

Figure 6(b). $\theta(\eta)$ Profiles for various M values.

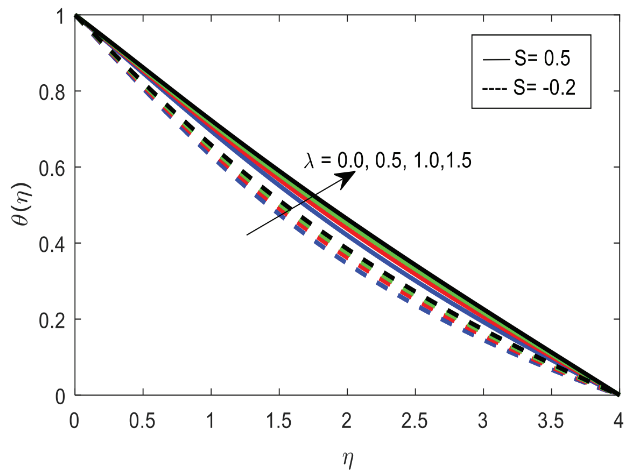

Figure 7(b). $\theta(\eta)$ Profiles for various λ values.

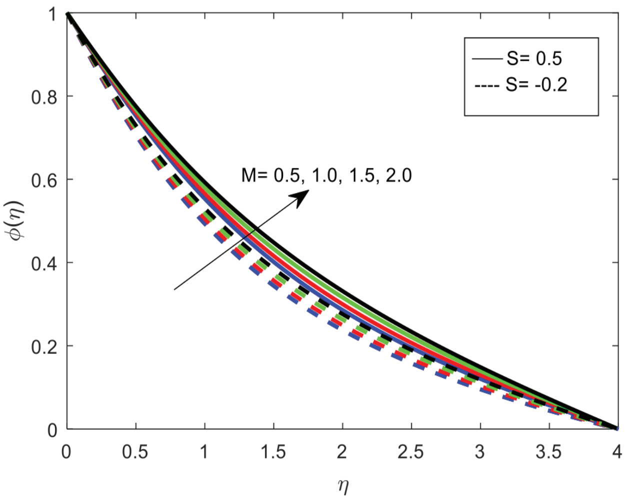

Figure 6(c). $\phi(\eta)$ Profiles for various M values.

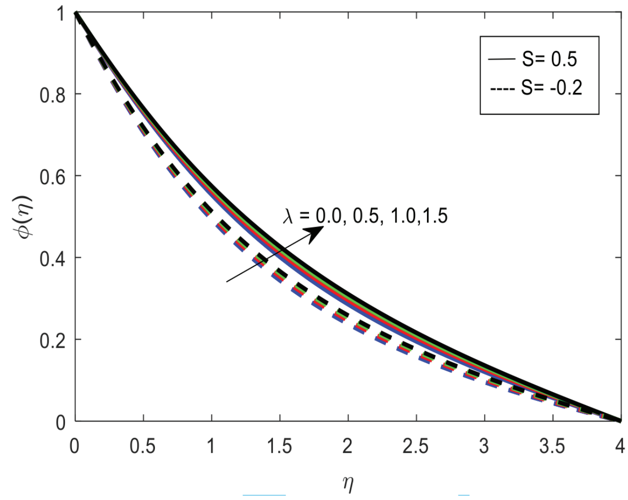

Figure 7(c). $\phi(\eta)$ Profiles for various λ values.

J Ther Eng, Vol. 11, No. 3, pp. 765−779, May, 2025

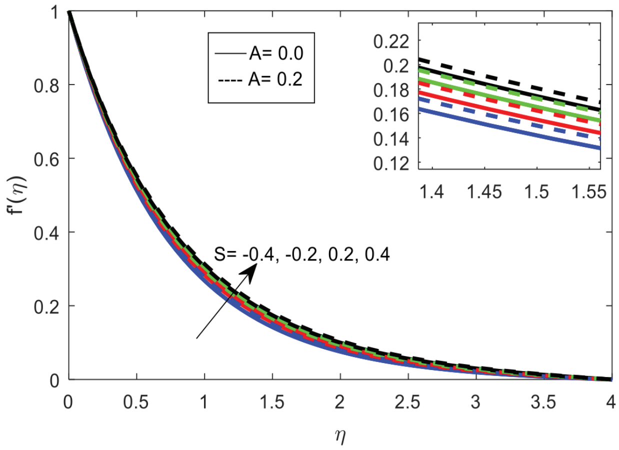

Figure 8(a). $f'(\eta)$ Profiles for various S values.

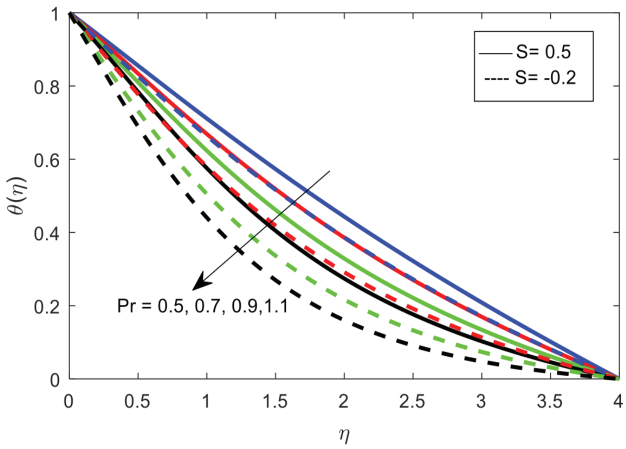

Figure 9(a). $\theta(\eta)$ Profiles for various Pr values.

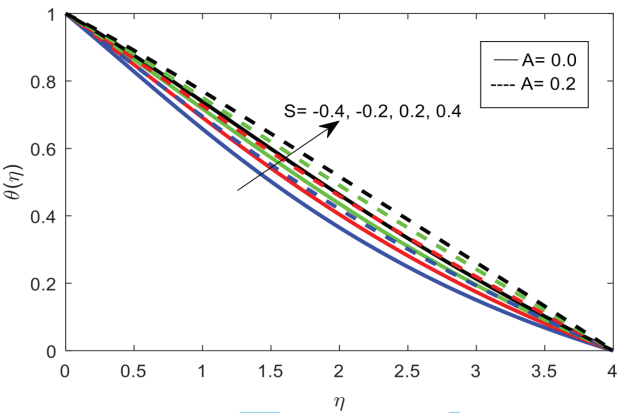

Figure 8(b). $\theta(\eta)$ Profiles for various S values.

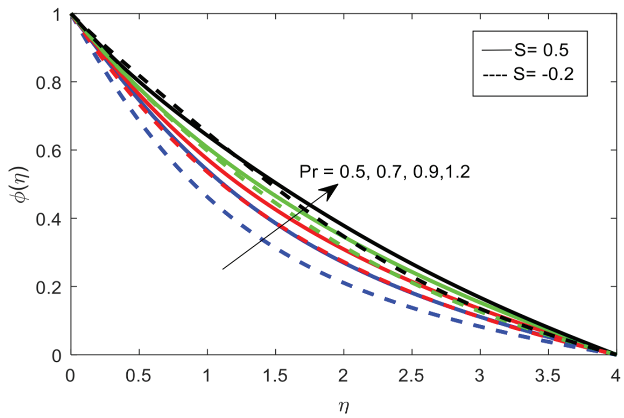

Figure 9(b). $\phi(\eta)$ Profiles for various Pr values.

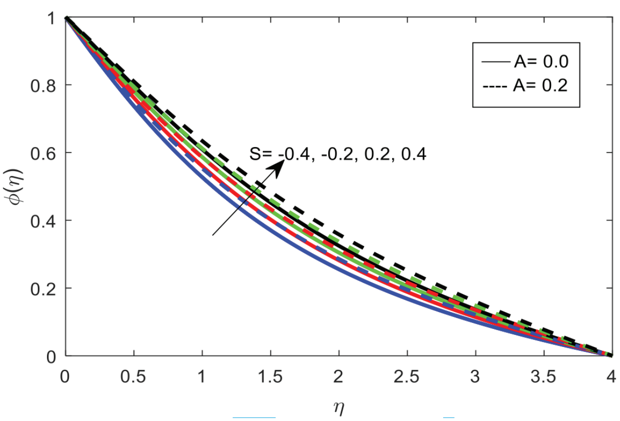

Figure 8(c). $\phi(\eta)$ Profiles for various S values.

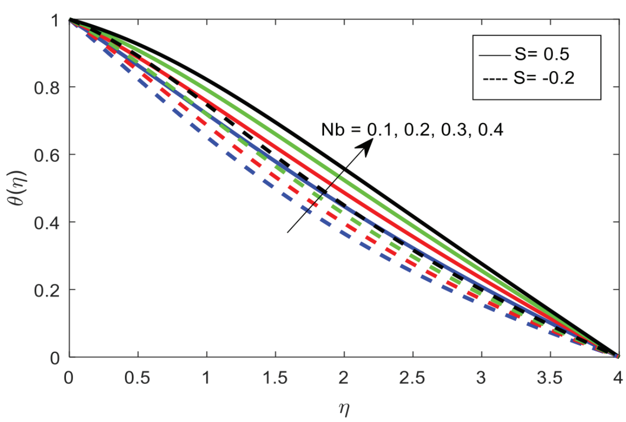

Figure 10(a). $\theta(\eta)$ Profiles for various Nb values.

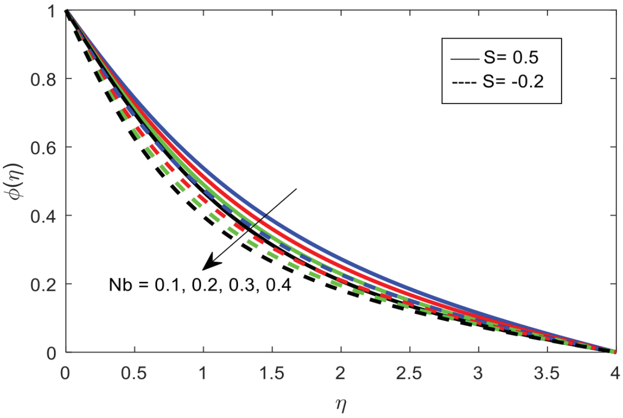

Figure 10(b). $\phi(\eta)$ Profiles for various *Nb* values.

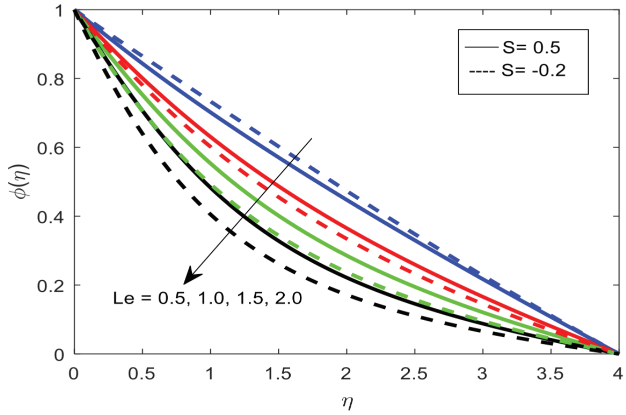

Figure 12. $\phi(\eta)$ Profiles for various *Le* values.

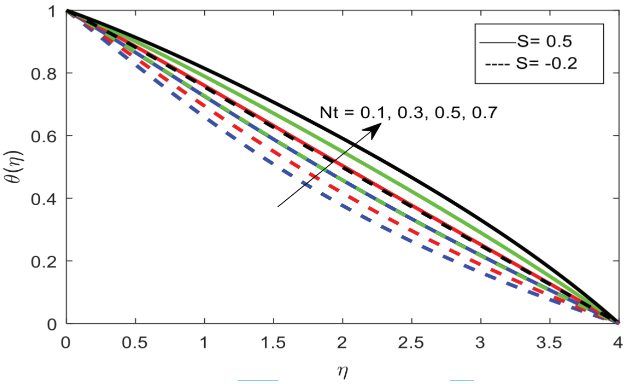

Figure 11(a). $\theta(\eta)$ Profiles for various *Nt* values.

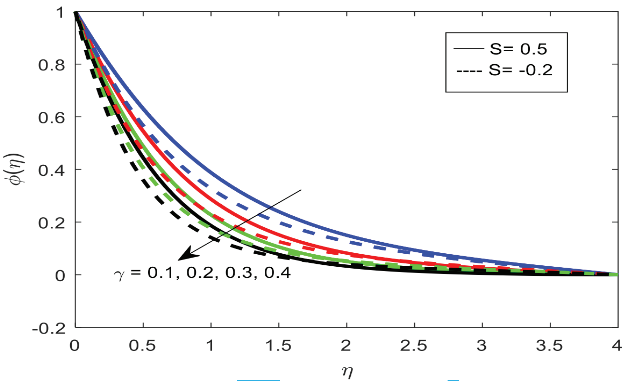

Figure 13. $\theta(\eta)$ Profiles for various γ values.

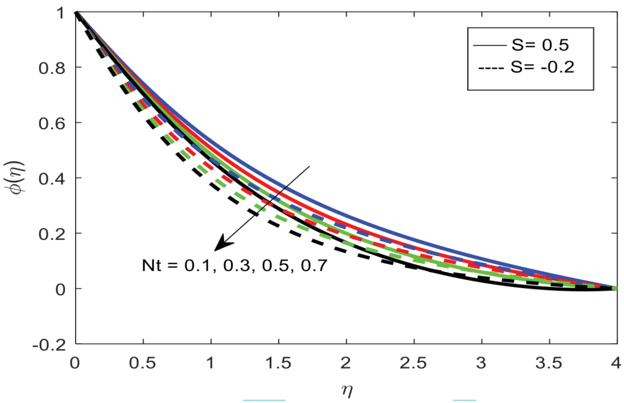

Figure 11(b). $\phi(\eta)$ Profiles for various *Nt* values.

CONCLUSION

"The physical aspects of the model used in the study of unsteady MHD Carreau nanofluid flow over a stretched surface in a porous medium with Stefan blowing condition encompass a variety of phenomena and interactions. In this study, we conducted a numerical analysis of the two-dimensional unsteady Stefan blowing influence on MHD Carreau nanofluid flow past a stretching sheet embedded in a porous medium. Our investigation focused on examining the characteristics of temperature, velocity, and concentration profiles through the use of graphical representations and tables. The key findings of our study can be summarized as follows:"

1. The velocity profile exhibited a simultaneous increase with the power law index, magnetic parameter, and porosity parameter in both the blowing and Stefan suction scenarios.
2. The velocity profiles demonstrated a decreasing trend as the Weissenberg number, unsteadiness parameter, and Stefan blowing/suction parameter increased.
3. Greater power law index, magnetic, unsteadiness, and porosity levels were found to result in amplified heat transmission.
4. The temperature profiles exhibited a decreasing trend as the Weissenberg number and Prandtl number increased, indicating enhanced heat dissipation.

Table 3. The values of skin friction coefficient, Nusselt number and Sherwood number for various values of *n, We, A, M, λ, S, Le, Pr, Nb, Nt, γ*

n	*We*	*A*	*M*	*λ*	*S*	*Le*	*Pr*	*Nb*	*Nt*	*γ*	$f''(0)$	$-\theta'(0)$	$-\phi'(0)$
0.1											-1.292206	0.345154	0.600737
0.2											-1.306662	0.344500	0.600090
	0.3										-1.357340	0.342381	0.597978
	0.4										-1.327668	0.343590	0.599186
		0.2									-1.357340	0.342381	0.597978
		0.3									-1.340922	0.320899	0.579035
			0.5								-1.357340	0.342381	0.597978
			1.0								-1.528992	0.325169	0.582945
				0.5							-1.357340	0.342381	0.597978
				0.7							-1.406403	0.337188	0.593504
					0.1						-1.357340	0.342381	0.597978
					0.2						-1.344765	0.329274	0.578626
						1.0					-1.355457	0.343494	0.454290
						1.5					-1.357340	0.342381	0.597978
							0.6				-1.357062	0.328450	0.610293
							0.7				-1.357340	0.342381	0.597978
								0.2			-1.357340	0.342381	0.597978
								0.3			-1.357062	0.327981	0.610272
									0.1		-1.357340	0.342381	0.597978
									0.2		-1.357106	0.330386	0.608324
										0.5	-1.357340	0.342381	0.597978
										1.0	-1.354635	0.337767	0.717874

5. Concentration profiles displayed an increase with higher values of the unsteadiness parameter, porosity parameter, and magnetic parameter, while they decreased with an increase in the Brownian motion, Lewis number, and chemical reaction parameters.
6. The skin friction coefficient, Nusselt number, and Sherwood number decreased with increasing power law index, magnetic parameter, and porosity parameter. However, the Weissenberg number exhibited the opposite trend."

These findings provide valuable insights into the complex interplay between various parameters in the MHD Carreau nanofluid flow with unsteady Stefan blowing. The results contribute to the understanding of heat transfer and fluid dynamics in porous media systems, which can have implications for the design and optimization of thermal management, cooling, and lubrication systems in numerous engineering applications. Further investigations can build upon these findings to explore additional aspects of the flow behavior and optimize the system›s performance.

NOMENCLATURE

x, y	Cartesian coordinates
u, v	Velocity components along *x and y* directions
a	Constant
A	Unsteadiness parameter
α	Thermal diffusivity
ν	Kinematic viscosity
B_0	Uniform magnetic field
ρ	Density
k	Thermal conductivity
k_1	Darcy permeability of the porous medium
μ	Dynamic viscosity
σ	Electrical conductivity
D_T	Thermophoretic diffusion coefficient
$(\rho c)_f$	Heat capacitance of nanofluid
$(\rho c)_p$	Heat capacitance of the nanoparticle
C	Nanoparticle volume fraction
C_∞	Concentration of the free stream
C_W	Concentration at the surface
C_T	Dimensional chemical reaction parameter
D_B	Brownian diffusion
T	Dimensional temperature of the fluid
T_W	Temperature at the surface
T_∞	Temperature of the free stream
Le	Lewis number
Re_x	Local Reynolds number
We	Weissenberg number
φ	Dimensionless nanoparticle volume fraction
C_p	Specific heat at constant pressure

ψ	Stream function
f	Dimensionless stream function
η	Similarity independent variable
M	Magnetic parameter
n	Power index number
Pr	Prandtl number
Γ	Positive time constant
Nt	Thermophoresis parameter
S	Suction/ injection
γ	Non-dimensional chemical reaction parameter
Nb	Brownian motion parameter
θ	Dimensionless temperature
ϕ	Dimensionless concentration function
λ	Porasity parameter
C_f	Skin friction coefficient
Nu	Nusselt number
Sh	Local Sherwood number

Subscripts

w	Condition at wall
∞	Condition at far away

AUTHORSHIP CONTRIBUTIONS

Authors equally contributed to this work.

DATA AVAILABILITY STATEMENT

The authors confirm that the data that supports the findings of this study are available within the article. Raw data that support the finding of this study are available from the corresponding author, upon reasonable request.

CONFLICT OF INTEREST

The authors declared no potential conflicts of interest with respect to the research, authorship, and/or publication of this article.

ETHICS

There are no ethical issues with the publication of this manuscript.

REFERENCES

[1] Sreeremya TS, Krishnan A, Mohamed P, Hareesh U, Ghosh S. Synthesis and characterization of cerium oxide based nanofluids: an efficient coolant in heat transport applications. Chem Eng J 2014;255:282–289. [CrossRef]

[2] Zarifi E, Jahanfarnia G, Veysi F. Sub-channel analysis of nanofluids application to VVER-1000 reactor. Chem Eng Res 2013;91:625–632. [CrossRef]

[3] Su F, Deng Y, Ma H. Numerical analysis of ammonia bubble absorption in a binary nanofluid. Chem Eng Comm 2015;202:500–507. [CrossRef]

[4] Tripathi D, Bég OA. Mathematical modeling of peristaltic pumping of nano-fluids. In: Basu SK, Kumar N. Modelling and Simulation of Diffusive Processes. Berlin/Heidelberg: Springer; 2014. pp. 69–95. [CrossRef]

[5] Khan SA, Nie Y, Ali B. Multiple slip effects on MHD unsteady viscoelastic nano-fluid flow over a permeable stretching sheet with radiation using the finite element method. SN Appl Sci 2020;2:1–14. [CrossRef]

[6] Liu L. Aggregation of silica nanoparticles in an aqueous suspension. AIChE J 2015;61:2136–46. [CrossRef]

[7] Ali B, Hussain S, Naqvi SIR, Habib D, Abdal S. Aligned magnetic and bio-convection effects on tangent hyperbolic nanofluid flow across faster/slower stretching wedge with activation energy: Finite element simulation. Int J Appl Comp Math 2020;7:1–20. [CrossRef]

[8] Ali B, Rasool G, Hussain S, Baleanu D, Bano S. Finite element study of magnetohydrodynamics (MHD) and activation energy in Darcy–Forchheimer rotating flow of Casson Carreau nanofluid. Processes (MDPI) 2020;8:1185. [CrossRef]

[9] Masuda H, Ebata A, Teramae K, Hishinuma N, Ebata Y. Alteration of thermal conductivity and viscosity of liquid by dispersing ultra-fine particles (dispersion of-Al2O3, SiO2 and TiO2 ultra-fine particles). Netsu Bussei 1993;7:227–233. [CrossRef]

[10] Choi S. Enhancing thermal conductivity of fluids with the nanoparticle. In: Development and Applications of Non-Newtonian Flow. ASME Fluids Eng Div 1995;231:99–105.

[11] Buongiorno J. Convective transport in nanofluids. J Heat Transf 2006;128:240–250. [CrossRef]

[12] Eastman JA, Phillpot S, Choi S, Keblinski P. Thermal transport in nanofluids. Annu Rev Mater Res 2004;34:219–246. [CrossRef]

[13] Khairul M, Shah K, Doroodchi E, Azizian R, Moghtaderi B. Effects of surfactant on stability and thermo-physical properties of metal oxide nanofluids. Int J Heat Mass Transf 2016;98:778–787. [CrossRef]

[14] Ali B, Nie Y, Hussain S, Habib D, Abdal S. Insight into the dynamics of fluid conveying tiny particles over a rotating surface subject to Cattaneo–Christov heat transfer, Coriolis force, and Arrhenius activation energy. Comp Math Appl 2021;93:130–143. [CrossRef]

[15] Bagherzadeh SA, Jalali E, Sarafraz MM, Akbari OA, Karimipour A, Goodarzi M, Bach QV. Effects of magnetic field on micro cross jet injection of dispersed nanoparticles in a microchannel. Int J Numer Methods Heat Fluid Flow 2019;30:2683–2704. [CrossRef]

[16] Khan ZH, Khan WA, Pop I. Triple diffusive free convection along a horizontal plate in porous media saturated by a nanofluid with convective boundary condition. Int Comm Heat Mass Transf 2013;66:603–612. [CrossRef]

[17] Krishna MV, Reddy GS. MHD forced convective flow of non-Newtonian fluid through stumpy permeable porous medium. Mater Today Proc 2018;5:175–183. [CrossRef]

[18] Hayat T, Qasim M, Mesloub S. MHD flow and heat transfer over permeable stretching sheet with slip conditions. Int J Numer Methods Fluids 2011;66:963–975. [CrossRef]

[19] Reddappa B, Geetha R. Effects of second order chemical reaction on MHD forced convection Cu, Ag, and Fe3O4 nanoparticles of Jeffrey Nanofluid over a moving plate in a porous medium in the presence of heat source/sink. J Integr Sci Technol 2023;12:1–10. [CrossRef]

[20] Reddappa B, Sudheer Babu M, Sreenadh S. Magneto-hydrodynamic (MHD) Jeffrey Nanofluid Flow over an Exponentially Stretching Sheet through a Porous Medium. AIP Conf Proc 2023;2649:1–16. [CrossRef]

[21] Ravikumar S, Ijaz Khan M, Reddappa B. The effects of diffusion on the mechanism of peristaltic flow at slip boundaries when internal Joule heating is present. Heat Transf 2023;52:1–28. [CrossRef]

[22] Sudheer Babu M, Reddappa B, Ajmath KA. Chemical Reaction Effects on MHD Heat and Mass Transfer of a Jeffrey Fluid Flow with Viscous Dissipation and Joule Heating Through a Porous Stretching Sheet. ARPN J Eng Appl Sci 2023;18:102–112. [CrossRef]

[23] Reddappa B, Sudheer Babu M, Sreenadh S, Durgaprasad P. The flow of non-Newtonian fluid in an inclined channel through variable permeability. Heat Transf 2023;52:3058–3073. [CrossRef]

[24] Reddappa B, Sudheer Babu M, Sreenadh S. MHD free convection and the effects of second order chemical reactions and double stratification jeffrey flow through porous medium over an exponentially stretching sheet. ARPN J Eng Appl Sci 2022;17:1047–1059.

[25] Ali N, Hayat T. Peristaltic motion of a Carreau fluid in an asymmetric channel. Appl Math Comp 2007;193:535–552. [CrossRef]

[26] Ali ME. The effect of lateral mass flux on the natural convection boundary layers induced by a heated vertical plate embedded in a saturated porous medium with internal heat generation. Int J Therm Sci 2007;46:157–163. [CrossRef]

[27] Hiemenz K. Die Grenzschicht an einem in den gleichformigen Flussigkeitsstrom eingetauchten geraden Kreiszylinder. Dingler›s Polytech J 1911;326:321–324.

[28] Abel S, Prasad KV, Mahaboob A. Buoyancy force and thermal radiation effects in MHD boundary layer visco-elastic fluid flow over continuously moving stretching surface. Int J Therm Sci 2005;44:465–476. [CrossRef]

[29] Olajuwon BI. Convection heat and mass transfer in a hydromagnetic Carreau fluid past a vertical porous plate in presence of thermal radiation and thermal diffusion. Therm Sci 2011;15:241–252. [CrossRef]

[30] Hayat T, Saleem N, Ali N. Effect of induced magnetic field on peristaltic transport of Carreau fluid. Comm Nonlinear Sci Numer Simul 2010;15:2407–2423. [CrossRef]

[31] Akbar NS, Nadeem S, Haq RU, Shiwei Y. MHD stagnation point flow of Carreau fluid toward a permeable shrinking sheet: Dual solutions. Ain Shams Eng J 2014;5:1233–1239. [CrossRef]

[32] Suneetha S, Gangadhar K. Thermal radiation effect on MHD stagnation point flow of a Carreau fluid with convective boundary condition. Open Sci J Math Appl 2015;3:121–127.

[33] Abou-Zeid MY. Numerical treatment of heat and mass transfer of MHD flow of Carreau fluid with diffusion and chemical reaction through a Non-Darcy porous medium. Open Math J 2009;2:22–35. [CrossRef]

[34] Akbar NS, Nadeem S, Khan ZH. Numerical simulation of peristaltic flow of a Carreau nanofluid in an asymmetric channel. Alex Eng J 2014;53:191–197. [CrossRef]

[35] Akbar NS, Nadeem S. Combined effects of heat and chemical reactions on the peristaltic flow of carreau fluid model in a diverging tube. Int J Non-Linear Mech 2011;67:1818–1832. [CrossRef]

[36] Nandeppanavar MM, Vajravelu K, SubhasAbel M, Siddalingappa MN. MHD flow and heat transfer over a stretching surface with variable thermal conductivity and partial slip. Meccanica 2013;48:1451–1464. [CrossRef]

[37] Chaim TC. Heat transfer in a fluid with variable thermal conductivity over a linearly stretching sheet. Acta Mech 1998;129:63–72. [CrossRef]

[38] Cortell R. Viscous flow and heat transfer over a nonlinearly stretching sheet. Appl Math Comp 2007;184:864–873. [CrossRef]

[39] Vyas P, Ranjan A. Dissipative MHD boundary-layer flow in a porous medium over a sheet stretching nonlinearly in the presence of radiation. Appl Math Sci 2010;4:3133–3142.

[40] Ali ME. On thermal boundary layer on a power-law stretched surface with suction or injection. Int J Heat Fluid Flow 1995;16:280–290. [CrossRef]

[41] Sheikholeslami M, Barzegar Gerdroodbary M, Shafee A, Tlili I. Hybrid nanoparticles dispersion into water inside a porous wavy tank involving magnetic force. J Therm Anal Calorim 2020;141:1993–1999. [CrossRef]

[42] Manh TD, Bahramkhoo M, Barzegar Gerdroodbary M, Nam ND, Tlili I. Investigation of nanomaterial flow through non-parallel plates. J Therm Anal Calorim 2021;143:3867–3875. [CrossRef]

[43] Manh TD, Abazari AM, Barzegar Gerdroodbary M, Nam ND, Moradi R, Babazadeh H. Computational simulation of variable magnetic force on heat characteristics of backward-facing step flow. J Therm Anal Calorim 2021;144:1585–1596. [CrossRef]

[44] Barzegar Gerdroodbary M. Application of neural network on heat transfer enhancement of magnetohydrodynamic nanofluid. Heat Transfer. 2019;49:197–212. [CrossRef]

[45] Man Y, Barzegar Gerdroodbary M. Influence of Lorentz forces on forced convection of nanofluid in a porous enclosure. J Porous Media 2024;27:15–25. [CrossRef]

[46] Tlili I, Moradi R, Barzegar Gerdroodbary M. Transient nanofluid squeezing cooling process using aluminum oxide nanoparticle. Int J Modern Phys C 2019;30:1950078. [CrossRef]

[47] Ghosh S, Mukhopadhyay S. MHD slip flow and heat transfer of Casson nanofluid over an exponentially stretching permeable sheet. Int J Automot Mech Eng 2014;14:4785–4804. [CrossRef]

[48] Dey S, Mukhopadhyay S, Begum M. Stefan flow of nanofluid and heat transport over a plate in company of Thompson and Troian slip and uniform shear flow. Force Mech 2022;9:100129. [CrossRef]

[49] Grubka LJ, Bobba KM. Heat transfer characteristics of a continuous, stretching surface with variable temperature. Heat Transf J 1985;107:248–250. [CrossRef]

[50] Konai S, Maiti H, Mukhopadhyay S. Influences of Stefan blowing on unsteady flow of Casson nanofluid past a stretching surface. Forces Mech 2023;12:100227. [CrossRef]

[51] Oyelakin IS, Mondal S, Sibanda P. Unsteady Casson nanofluid flow over a stretching sheet with thermal radiation, convective and slip boundary conditions. Alex Eng J 2016;55:1025–1035. [CrossRef]

[52] Sharidan S, Mahmood T, Pop I. Similarity solutions for the unsteady boundary layer flow and heat transfer due to a stretching sheet. Int J Appl Mech Eng 2006;11:647–654.

[53] Mukhopadhyay S, De PR, Bhattacharyya K, Layek GC. Casson fluid flow over an unsteady stretching surface. Ain Shams Eng J 2013;4:933–938. [CrossRef]

[54] Konai S, Maiti H, Mukhopadhyay S. Influences of Stefan blowing on unsteady flow of Casson nanofluid past a stretching surface. Forces Mech 2023;12:100227. [CrossRef]